



Scaling law in the inviscid coalescence of unequal-size droplets

Xi Xia^{1,†} , Yicheng Chi^{2,3,†} and Peng Zhang²

¹School of Mechanical Engineering, Shanghai Jiao Tong University, Shanghai 200240, PR China

²Department of Mechanical Engineering, City University of Hong Kong, Kowloon Tong 999077, Hong Kong

³School of Automotive and Transportation Engineering, Shenzhen Polytechnic University, Shenzhen 518055, PR China

Corresponding author: Peng Zhang, penzhang@cityu.edu.hk

(Received 18 January 2025; revised 24 February 2025; accepted 23 March 2025)

Droplet coalescence is an essential multiphase flow process in nature and industry. For the inviscid coalescence of two spherical droplets, our experiment shows that the classical $1/2$ power-law scaling for equal-size droplets still holds for the unequal-size situation of small size ratios, but it diverges as the size ratio increases. Employing an energy balance analysis, we develop the first theory for asymmetric droplet coalescence, yielding a solution that collapses all experimental data of different size ratios. This confirms the physical relevance of the new set of length and time scales given by the theory. The functionality of the solution reveals an exponential dependence of the bridge's radial growth on time, implying a scaling-free nature. Nevertheless, the small-time asymptote of the model is able to recover the classical power-law scaling, so that the actual bridge evolution still follows the scaling law asymptotically in a wide parameter space. Further analysis suggests that the scaling-free evolution behaviour emerges only at late coalescence time and large size ratios.

Key words: breakup/coalescence

1. Introduction

Droplet coalescence (Eggers, Lister & Stone 1999; Aarts *et al.* 2005; Kavehpour 2015; Eggers, Sprittles & Snoeijer 2025) ubiquitously exists in numerous natural and industrial processes, such as rain drop formation (Grabowski & Wang 2013), fuel spray (Qian & Law 1997), sintering (Pokluda, Bellehumeur & Vlachopoulos 1997), emulsions

[†]These two authors contributed equally.

(Keiser *et al.* 2017), inkjet printing (Lohse 2022), etc. The coalescence commences upon the initial contact or impact of droplets, followed by the formation of a thin liquid bridge between the two merging liquid–gas interfaces. The liquid bridge then undergoes a rapid outward expansion, driven by a large capillary pressure (or surface tension) exerted on the high-curvature bridge interface.

Extensive interest has been drawn to understand such a coalescence motion in the most basic situation – the momentumless coalescence of a pair of liquid droplets (Eggers *et al.* 1999; Aarts *et al.* 2005; Thoroddsen, Takehara & Etoh 2005; Paulsen, Burton & Nagel 2011; Zhang & Law 2011; Paulsen *et al.* 2014; Kavehpour 2015; Eggers *et al.* 2025). To describe the liquid-bridge evolution in the inviscid (or inertial) regime, where the liquid–gas interface movement is dominated by a balanced effect between surface tension and fluid inertia, Eggers *et al.* (1999) first derived the well-known scaling theory of $R \sim t^{1/2}$ between the liquid-bridge radius R and time t . This $1/2$ power-law scaling was later corroborated by numerous experimental (Wu, Cubaud & Ho 2004; Aarts *et al.* 2005; Thoroddsen *et al.* 2005; Fezzaa & Wang 2008; Case 2009) and numerical (Duchemin, Eggers & Josseran 2003; Burton & Taborek 2007; Pothier & Lewis 2012; Sprittles & Shikhmurzaev 2012; Gross *et al.* 2013) studies. On the other hand, the bridge evolution is better modeled by a linear scaling (Aarts *et al.* 2005; Thoroddsen *et al.* 2005; Yao *et al.* 2005; Burton & Taborek 2007; Paulsen *et al.* 2011) in the viscous regime, where the surface tension serves to overcome the viscous stress. The crossover (or transition) (Burton & Taborek 2007) between the viscous and inertial regimes has also attracted considerable interest, from the discovery of a master curve for both regimes (Paulsen *et al.* 2011; Paulsen 2013) to the development of theoretical models justifying the underlying universality (Xia, He & Zhang 2019; Hack *et al.* 2020).

Previous research on binary droplet coalescence revolves mainly around two equal-size droplets. However, less attention has been given to droplet coalescence with size disparities, despite its higher relevance to reality. Among the existing works involving the coalescence of unequal-size droplets (Anilkumar, Lee & Wang 1991; Blanchette 2010; Liu *et al.* 2013; Sun *et al.* 2015; Tang *et al.* 2016; Xia *et al.* 2017; Ray *et al.* 2023), the main focus was on the effect of internal mixing or the coalescence outcome facilitated by the breaking of symmetry. Regarding the evolution of the liquid bridge, it is evident from our previous work (Xia *et al.* 2017) that the bridge surface shows an asymmetric growth – the bridge interface becomes tilted as it expands out. Yet, little quantitative study exists on the liquid-bridge evolution of unequal-size droplet coalescence. Especially, an intriguing question is whether a scaling law still exists in the asymmetric coalescence scenario.

In this work, we first conduct an experiment to resolve the bridge’s evolution process of droplet coalescence for various size ratios. Then, based on understanding the liquid-bridge configuration, we obtain several key correlations of the bridge’s geometry by assuming ‘small bridge’ and ‘arc-shaped bridge interface’. Further employing an energy balance analysis, we are able to derive the first analytical solution for the radial movement of the liquid bridge between two coalescing droplets of distinct sizes. The performance of this model is testified through the comparison with experimental data.

2. Experimental approach and observations

To have a basic understanding of the coalescence of two unequal-size droplets, we first conduct an experiment to resolve the bridge’s temporal evolution for droplet pairs of various liquid properties and size ratios. Our experiment employs the classical sessile-pendant approach for droplet coalescence, similar to those reported previously (Aarts *et al.* 2005; Thoroddsen *et al.* 2005; Fezzaa & Wang 2008; Case 2009). A schematic of the set-up is illustrated in figure 1(a). During each experimental run, a sessile droplet

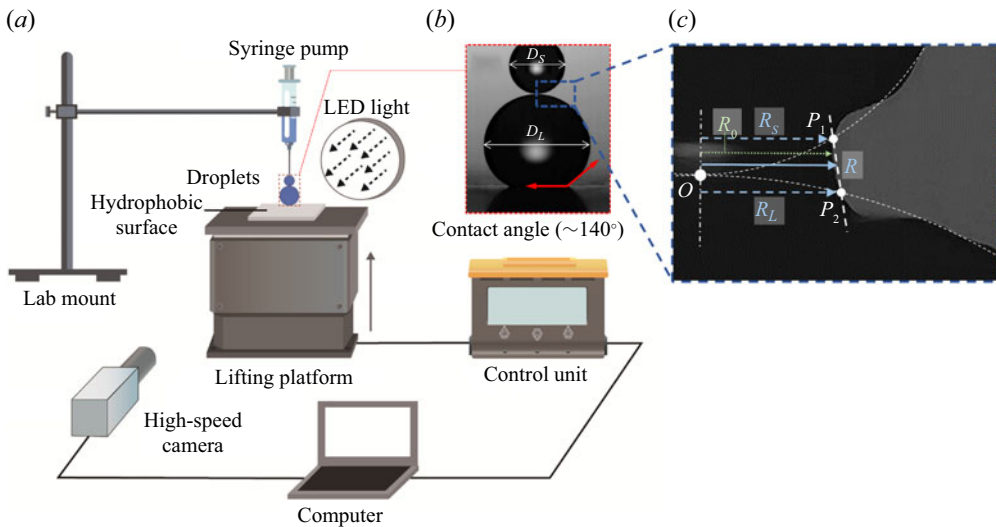


Figure 1. (a) Schematic of the experimental set-up, (b) image of a pair of sessile and pendant droplets, and (c) zoomed-in detail of the liquid bridge. Here, P_1 and P_2 are the intersection points corresponding to the two characteristic radii, R_S and R_L .

with a diameter of 1–6 mm is first generated by a syringe pump (Longer Precision Pump) and placed on a super-hydrophobic surface (acrylic coated with a mixture of nano silica, silicone resin and ethanol), yielding a contact angle of $\sim 140^\circ$ and a near-spherical upper part as depicted in figure 1(b). Then, the syringe pump generates a smaller-size pendant droplet (1–2 mm in diameter), which is attached to the needle tip. The size disparity is quantified by the droplet size ratio, $\Delta = D_L/D_S$, where D_S and D_L are the diameters of the small and large droplets, respectively. In this experiment, the variation range of Δ is between 1.0 and 5.0. Subsequently, the merging process is initiated by actuating an automatic lifting platform (Winner Optics) which holds the super-hydrophobic surface, slowly bringing the sessile droplet into contact with the pendant droplet. The platform rises at a quite low speed of approximately $10 \mu\text{m s}^{-1}$ so that the gas-film flow has a negligible influence on the initial droplet coalescence (Case & Nagel 2008; Case 2009; Paulsen *et al.* 2011). Based on the work of Zhang & Law (2011), the van der Waals force driving the interface merging becomes dominant when the gap (h) between the two interfaces closes down to $O(10^{-8})$ m. Based on their theory, the gas-film pressure of this experiment is estimated to be $O(10)$ Pa for $h = 10^{-8}$ m, which is much smaller than the capillary pressure of $O(10^2)$ Pa; this means that the gas-film pressure is too small to cause significant interface deformation prior to the coalescence onset.

A high-speed camera (Photron SA-Z) integrated with a long-distance microscope (Quesar QM100) is used to capture time-resolved shadowgraph images of the merging droplets. The camera operates at 150 000 frames per second (f.p.s.) with a spatial resolution of 384×256 pixels and a field of view of $2.04 \times 1.36 \text{ mm}^2$, corresponding to a resolution of $5.3 \mu\text{m pixel}^{-1}$. The initial time for the coalescence onset is defined based on the first frame showing apparent droplet contact and formation of a liquid bridge. As the shutter speed is set at $1/197\,647$ s, this yields an uncertainty of $\pm 2.53 \times 10^{-6}$ s in measuring the coalescence time. The droplet diameter is determined at the initial state prior to the coalescence, based on fitting an arc to three arbitrarily selected points on each droplet contour. The uncertainty associated with the diameter measurement is estimated to be within $\pm 3\%$.

Parameters	Water						40 wt % Glycerol				60 wt % Glycerol			
D_L (mm)	1.98	2.20	2.84	4.90	5.60	4.07	4.19	4.31	3.31	6.11	6.47	3.09	4.75	3.38
D_S (mm)	1.90	1.93	1.76	1.79	1.72	1.06	1.00	0.87	2.16	2.15	1.97	1.97	1.81	1.07
Δ	1.0	1.1	1.6	2.7	3.3	3.8	4.2	5.0	1.5	2.8	3.3	1.6	2.6	3.2
Oh ($\times 10^{-3}$)	2.7	2.7	2.8	2.8	2.8	3.6	3.7	4.0	8.9	8.9	9.3	27.9	29.1	37.9

Table 1. Parameters (D_L , D_S , Δ and Oh) of all experimental cases, sorted in ascending order of Δ for each fluid type. Note that two significant digits are adopted in the actual Δ calculations, e.g. $\Delta = 1.0$ should be 1.04.

Next, the radius of the liquid bridge is defined based on the experimental image. Figure 1(c) illustrates the zoomed-in detail of a representative liquid bridge, exhibiting a distinct asymmetric bridge interface. As such, we can define two characteristic radii of the droplet bridge, R_S and R_L , respectively as the radial distances from the two points, P_1 and P_2 , where the bridge interface intersects the contours of the initial droplets (denoted by the white-dashed lines), to the axis of symmetry. Then, the characteristic radius of the circular bridge, R , is defined as $R = (R_S + R_L)/2$. Considering the uncertainties in estimating the initial droplet diameters, the error propagates in determining the intersection points P_1 and P_2 , yielding an uncertainty in the range of $\pm 0.1\%$ to $\pm 1\%$ in the R calculation. Note the definition of R differs from the equal-size situation, for which the bridge radius is typically defined as the minimum radial distance of the bridge interface to the centre axis, marked by R_0 in figure 1(c). Given the concave shape of the interface, R is slightly larger than R_0 in the unequal-size coalescence (see figure S1 of the supplementary material for a quantitative comparison available at <https://doi.org/10.1017/jfm.2025.353>).

To account for the effect of varying liquid properties, i.e. density ρ_l , dynamic viscosity μ_l and surface tension σ , we adopt water and two aqueous glycerol solutions with 40 wt % and 60 wt % glycerol. These liquids correspond to $\rho = 1000, 1100$ and 1150 kg m^{-3} , $\mu = 1.002, 3.630$ and 10.80 mPa s , and $\sigma = 72.8, 70.0$ and 66.0 mN m^{-1} , respectively. The different liquids can be characterised by the non-dimensional Ohnesorge number, $Oh = \mu_l(\rho_l \sigma D_S)^{-1/2}$. In this experiment, Oh varies in the range of 10^{-3} – 10^{-2} , which belongs to the inviscid or inertia coalescence regime (Xia *et al.* 2019). The test parameters for all cases are characterised in terms of Δ and Oh , as listed in table 1. The corresponding coalescence images are included in figures S2–S4 of the supplementary material.

The image sequences for representative droplet coalescence cases are presented in figure 2(a–c), where the droplet interface contours corresponding to the different snapshots are extracted and overlapped in figure 2(d–f). We observe from figures 2(e) and 2(f) that the liquid bridge displays a notable asymmetry for $\Delta > 1$, rendering an inclined bridge interface with $R_L > R_S$, which becomes more prominent as the bridge expands. As Oh increases from 0.0028 to 0.0093, the bridge profiles in figure 2(f) follow the original droplet contour more closely than those in figure 2(e), as the ripple-like structures on the bridge’s upper and lower surfaces tend to be inhibited. These ripples can be understood as capillary waves developing along the droplet surface, owing to the perturbation of the radially expanding liquid bridge, which can be damped by enhanced viscosity.

3. Theoretical model

3.1. Assumptions and correlations

To understand the distinct scaling behaviours in unequal-size droplet coalescence, we next introduce a model for two merging droplets of different but comparable sizes

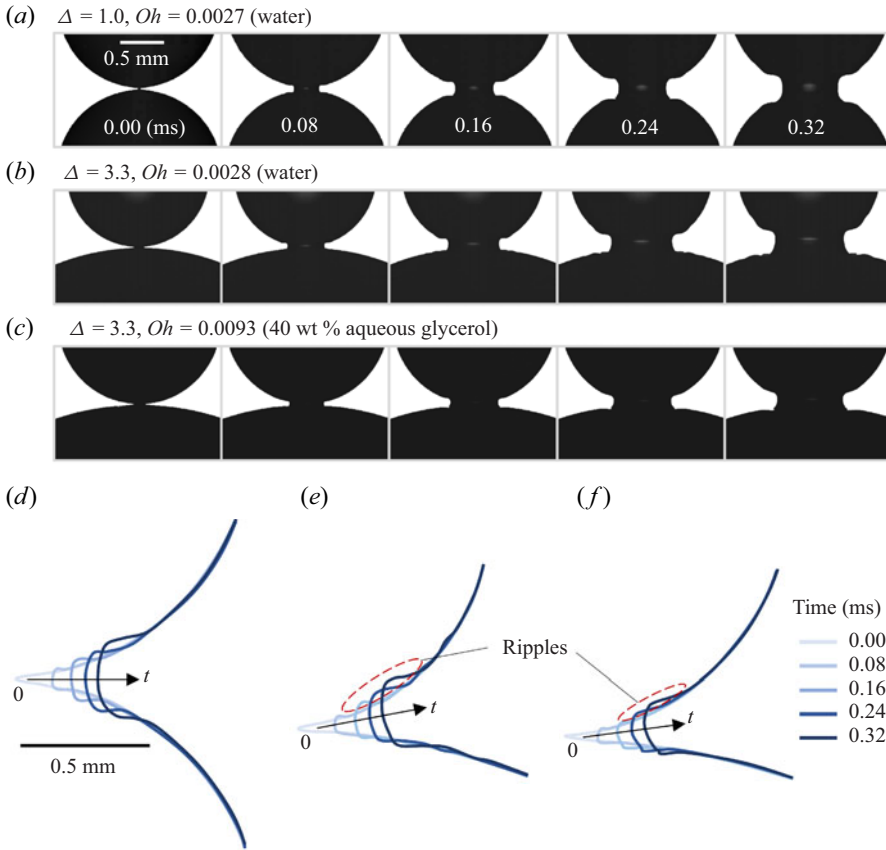


Figure 2. (a–c) Image sequences of the droplet coalescence process of three different cases and (d–f) evolutions of the liquid-bridge contours extracted from the images in (a–c), respectively.

(i.e. $\Delta \sim O(1)$, $R_L/R_S \sim O(1)$ and $\theta_L/\theta_S \sim O(1)$). A simplified geometry of the liquid-bridge interface is presented in figure 3(a), based on which two physical assumptions can be made.

(i) ‘small bridge’, meaning that the characteristic radii of the bridge, R_S and R_L , are much smaller than the droplet diameters, i.e. $R_S/D_S \sim o(1)$ and $R_L/D_L \sim o(1)$. This is clearly satisfied during the early-stage coalescence.

(ii) ‘arc-shaped bridge interface’, meaning the interface section between P_1 and P_2 can be approximated by an arc of the same curvature, where the pressure difference Δp is evenly distributed. As such, we can define the bridge’s principle normal direction \mathbf{n}_p as that pointing from the arc midpoint to the arc centre. This assumption can be considered a reasonable first approximation.

Several geometric correlations can be deduced from the coalescence model in figure 3(a). We begin with two basic ones:

$$\begin{aligned}
 R_S/D_S &= \frac{1}{2} \sin(2\theta_S) = \theta_S - O(\theta_S^3), \\
 R_L/D_L &= \frac{1}{2} \sin(2\theta_L) = \theta_L - O(\theta_L^3).
 \end{aligned}
 \tag{3.1}$$

Under assumption (i), both θ_S and θ_L are of $o(1)$, so the higher-order terms in (3.1) can be neglected.

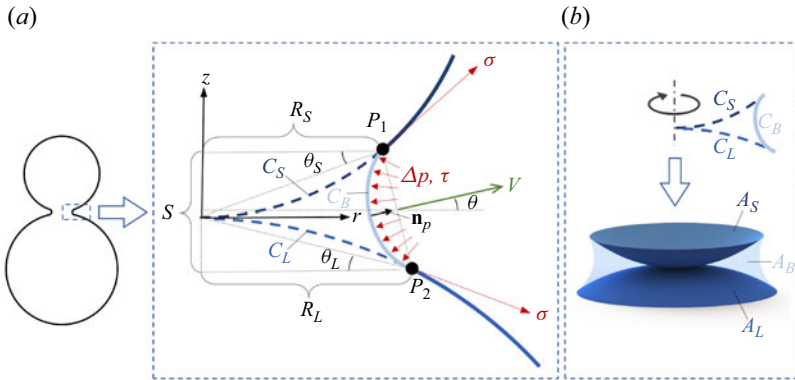


Figure 3. (a) Zoomed-in schematics of the liquid-bridge interface between two unequal-size merging droplets. The red arrows represent the forces applied over the bridge interface, and the green arrow indicates the overall movement of the interface. (b) Three main surfaces (A_S , A_L and A_B) with significant area changes, respectively corresponding to the three arc segments, C_S , C_L and C_B , in (a).

A key characteristic of the unequal-size coalescence, which differs from the equal-size situation, is the tilted bridge interface and the misaligned bridge movement from the radial direction, as delineated in figure 3(a). This tilted interface results from the force balance across the interface. Given the arc shape of the bridge interface according to assumption (ii), the total surface stress ($\Delta p + \tau$) has a symmetric distribution with respect to the arc midpoint, where $\tau = 2\mu \mathbf{S}$ is the viscous stress (\mathbf{S} is the strain-rate tensor). So the bridge's principle normal direction \mathbf{n}_p is in line with the integral of the total surface stress over the bridge interface, which is balanced by the surface tension σ pulling at its both ends (P_1 and P_2). Since the two surface tensions are of the same magnitude, \mathbf{n}_p must also be in line with the angular bisector of these two forces. Accordingly, the tilting angle (θ) of the bridge interface satisfies a simple geometric correlation:

$$\theta = \theta_S - \theta_L. \tag{3.2}$$

As θ_S and θ_L are of $o(1)$, θ is also of $o(1)$ and is thereby treated as the ‘small parameter’ in this model.

The width of the bridge (S), defined as the axial distance between P_1 and P_2 , has the correlation

$$S \approx R_S \theta_S + R_L \theta_L. \tag{3.3}$$

Furthermore, the interface geometry in figure 3(a) satisfies $R_L - R_S = S \tan \theta \approx S\theta$, which can be used to derive (3.2) and (3.3) as

$$\theta \approx \left(D_S^{-1} - D_L^{-1} \right) R, \tag{3.4}$$

$$S \approx \left(D_S^{-1} + D_L^{-1} \right) R^2. \tag{3.5}$$

The detailed derivations of (3.3)–(3.5) are provided in the supplementary material.

With the symmetrically distributed total surface stress and the evenly distributed Δp over the arc-shaped bridge interface (assumption (ii)) in figure 3(a), it can be implied that the viscous stress (τ) also has a symmetric distribution with respect to the arc midpoint. It follows that the liquid-side velocity must also be symmetrically distributed over the bridge interface, so that the overall bridge movement is in line with its principle normal direction \mathbf{n}_p . This has significant physical implications. Consider the very early stage of coalescence when $R_S \approx R_L$, (3.4) dictates that θ is a positive value. This explains why

the bridge movement is inclined towards the smaller droplet and why R_S is smaller than R_L from the beginning. Thus, the bridge interface movement can be described by an essential kinematic relationship, $dR/dt = V \cos \theta$, where V is the velocity at which the bridge interface expands radially. Applying Taylor expansion, it takes the form

$$\frac{dR}{dt} \approx V \left(1 - \frac{\theta^2}{2} \right). \tag{3.6}$$

Note that (3.6) recovers the equal-size coalescence kinematics with vanishing θ .

3.2. Energy balance analysis

From the energy conservation perspective, the movement of the liquid entrained by the expanding bridge is driven by the rapid discharge of the surface energy, which can be formulated as $\Delta E_s + \Delta E_k \approx 0$, where ΔE_s and ΔE_k , respectively, represent the changes in surface and kinetic energies from the initial state of coalescence onset. Note this only applies to the inviscid-dominant regime ($Oh \sim o(1)$) with negligible viscous dissipation, which is valid for the present experiment.

According to figure 3(b), the change in surface energy can be estimated as $\Delta E_s = (-A_S - A_L + A_B)\sigma$, where A_S , A_L and A_B are the main surfaces with varying areas. It can be further derived as

$$\Delta E_s \approx -\pi D_S^2 \theta_S^2 \sigma - \pi D_L^2 \theta_L^2 \sigma + \pi S(R_S + R_L)\sigma, \tag{3.7}$$

where the third term is one order smaller than the first two terms and can be dropped off (see supplementary material for details). Additionally, ΔE_k can be estimated as

$$\Delta E_k \approx \frac{C}{2} \pi \rho_l R^2 S V^2, \tag{3.8}$$

where C is a prefactor related to the flow entrainment by the liquid bridge. Equations (3.7) and (3.8) are almost identical to those for the equal-size scenario, except for the terms relating to the size disparity.

With S and V given by (3.5) and (3.6), respectively, we can apply (3.7) and (3.8) to derive the energy balance as

$$\frac{1}{1 - \beta R^2/2} \frac{dR}{dt} \approx \frac{\gamma}{R}, \tag{3.9}$$

where $\beta = (D_S^{-1} - D_L^{-1})^2$ and $\gamma = (4\sigma D_S)^{1/2} [C\rho_l(1 + \Delta^{-1})]^{-1/2}$. Given the initial condition $R(t=0) = 0$, (3.9) has the solution, $R^2 \approx (2 - 2e^{-\beta\gamma t})\beta^{-1}$, with the non-dimensional form

$$R^{*2} \approx 2 - 2e^{-t^*}, \tag{3.10}$$

where $R^* = R\beta^{1/2}$ and $t^* = t\beta\gamma$. Interestingly, the bridge evolution governed by (3.10) no longer has a power-law scaling between R and t .

It is worth discussing the features of this solution. Letting $\Delta \rightarrow 1$ in (3.10), we have $\beta \rightarrow 0$ and $R^2 \approx 2[1 - (1 - \beta\gamma t)]/\beta = 2\gamma t$. This means that the present model is able to recover the inviscid scaling law of $R \sim t^{1/2}$ in the equal-size limit. Likewise, we attain $R^{*2} \approx 2t^*$ when $t^* \rightarrow 0$, suggesting that in practice the power-law scaling still holds for the early-stage coalescence of unequal-size droplets, owing to the asymmetric effect being negligible. When $t^* \rightarrow \infty$, it predicts $R^{*2} \approx 2$, which corresponds to an up-limit radius as if the bridge movement could turn continuously from radial to axial. It should be noted, however, the limiting R in reality is confined by the actual droplet sizes.

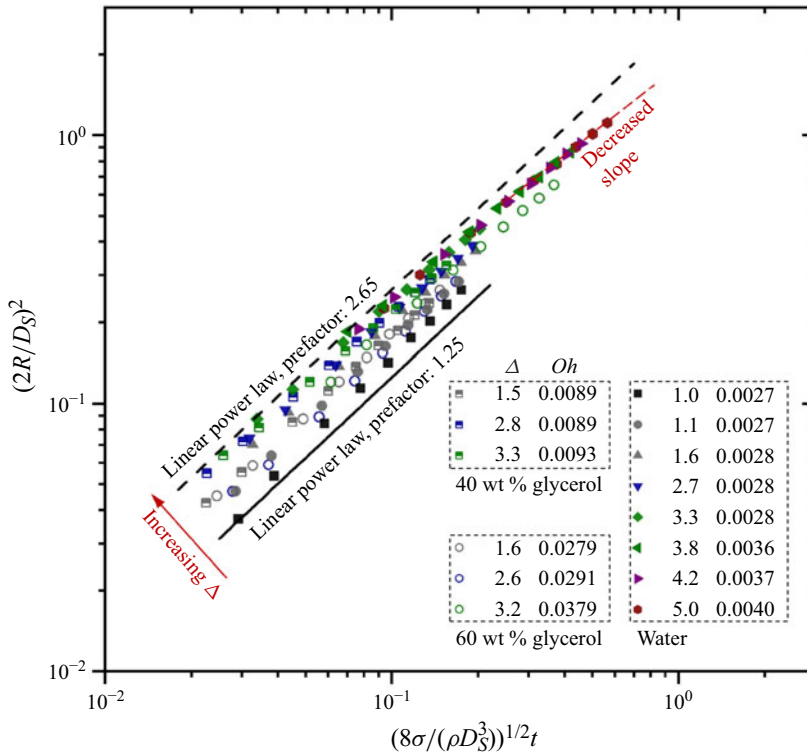


Figure 4. Effect of Δ on the scaling of $R^2 \sim t$. The bridge evolution images for all cases are reported in the supplementary material.

3.3. Model validation and discussion

Before verifying the proposed theory, we first check whether the classical scaling law of $R \sim t^{1/2}$ holds for unequal-size droplet coalescence, by plotting the time sequence data of the liquid-bridge radius for various Δ and Oh in the parameter space $[(8\sigma/(\rho D_S^3))^{1/2}t, (2R/D_S)^2]$ (Duchemin *et al.* 2003; Aarts *et al.* 2005) in figure 4. The result indicates that the $R^2 \sim t$ scaling is approximately valid for most cases. However, as Δ increases, there is an apparent upward drift of data from the baseline of $\Delta = 1.0$, which is associated with an increase of the scaling prefactor from 1.25 to 2.65. Note that, in terms of the scaling relation of $R \sim t^{1/2}$, where R is scaled by $D_S/2$ and t is scaled by $\tau_i = (\rho D_S^3/(8\sigma))^{1/2}$, the two corresponding prefactors are 1.12 and 1.63, respectively. The latter, marking the up-limit of the large- Δ cases, is significantly higher than those reported in previous equal-size experiments (Aarts *et al.* 2005). This can be physically understood in that the presence of a larger droplet enhances the expansion speed of the bridge interface. Furthermore, the cases with $\Delta > 3$ display slightly decreased slopes compared with that of $R^2 \sim t$ as time proceeds to the later stage of coalescence when the liquid bridge becomes more asymmetric, indicating a tendency to divert from the classical scaling of $R^2 \sim t$.

The comparison of the new theoretical model with the same data in figure 4 is presented in figure 5(a). We can observe the collapse of non-unity- Δ data onto a single line given by (3.10), with $C = 6$ given by fitting. In the equal-size limit ($\Delta \rightarrow 1$), $C = 6$ corresponds to a prefactor of 1.28 in the scaling relation of $R \sim t^{1/2}$ under the aforementioned non-dimensionalisation. This prefactor is in approximate agreement with previous experimental results, e.g. 1.03–1.29 in Wu *et al.* (2004) and 1.11–1.24 in

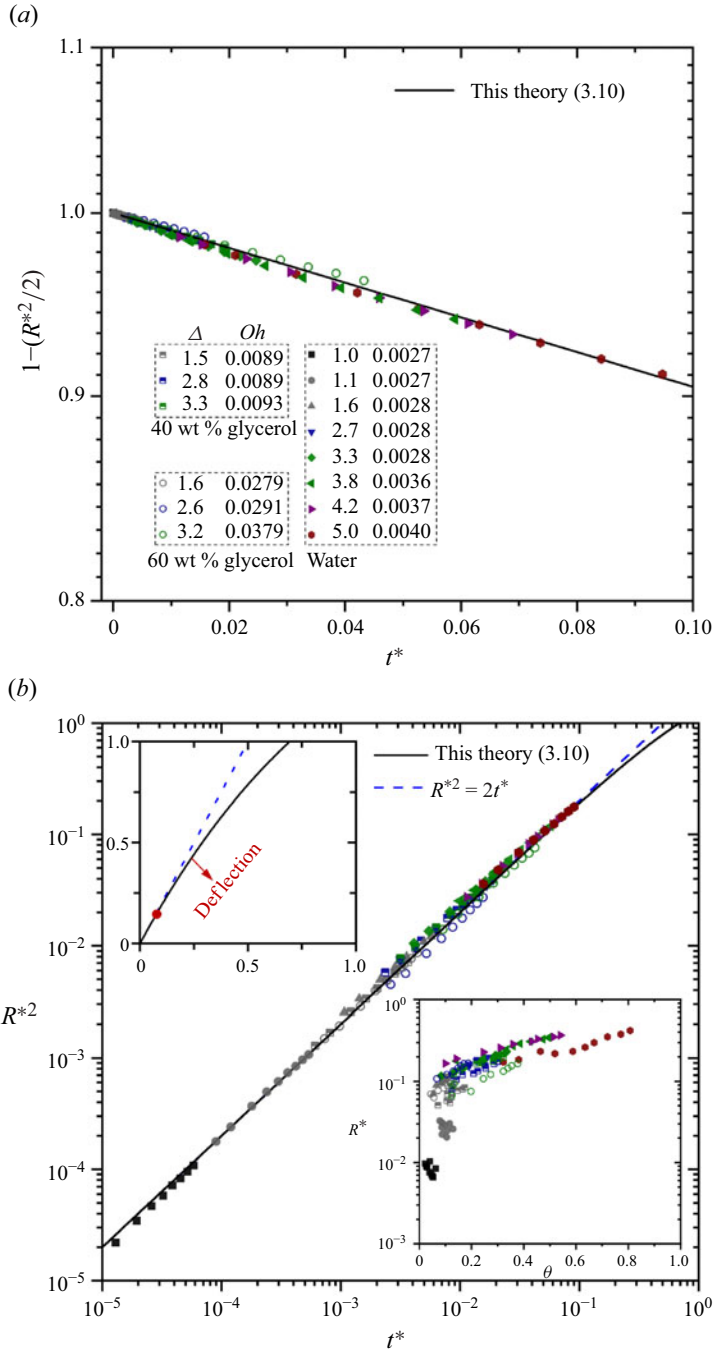


Figure 5. (a) Model validation of (3.10) against experimental data and (b) the performance of (3.10) versus the classical power-law scaling. The top-left inset in (b) shows the deflection of this model from the scaling law in normal coordinates; the bottom-right inset plots the experimental relationship between R^* and θ .

Aarts *et al.* (2005), which is supportive of our experimental data and model. In this sense, a major significance of the present work lies in its generalisation of Eggers *et al.* (1999)'s model through the consideration of droplet size disparity. However, it should be noted that this prefactor is slightly smaller than the numerical results, e.g. 1.62 in Duchemin *et al.* (2003) and 1.5 in Sprittles & Shikhmurzaev (2014). While further study is necessary, the discrepancy between experiment and simulation is possibly related to the ideal initial conditions of the simulations, which does not account for the van der Waals force or potential viscous effect that may influence the initial coalescence behaviours in reality.

Figure 5(a) justifies the universality of our theory in resolving the droplet coalescence of various size ratios, including the late-stage coalescence dynamics at large size ratios. Another important implication is that this theory offers the proper characteristic length and time scales for unequal-size droplet coalescence; these turn out to be $\beta^{-1/2}$ and $(\beta\gamma)^{-1}$, respectively, both of which depend on the size ratio Δ . So a larger Δ corresponds to larger R^* . The good agreement in figure 5(a) also suggests that although the theory was developed for the early-stage coalescence, which generally requires $R/D_S \sim o(1)$ according to assumption (i), the model prediction is potentially useful towards a much later stage—a typical observation in asymptotic analysis (Van Dyke 1964). This likely reflects that the geometric and kinematic correlations used in our model offer relatively accurate approximations to later stages. Nevertheless, the extension of this model to very late coalescence stages (R/D_S approaching 0.5) for large-size-ratio cases should be handled with caution, owing to the non-negligible errors associated with the finite bridge size as well as significant deviation from symmetry.

To assess to what extent the unequal-size droplet coalescence deviates from the power-law scaling of the equal-size case, figure 5(b) compares the data with (3.10) in the $R^{*2}-t^*$ diagram. Again, a promising agreement between experiment and theory can be confirmed; an uncertainty analysis is included in the supplementary material. However, the theoretical line here remains almost linear when $R^{*2} < 10^{-1}$, while it exhibits a slight deflection or deviation from the power-law scaling of $R^{*2} = 2t^*$ when $R^{*2} > 0.1$ or $R^* > 0.3$. According to the present study, this deviation can be interpreted as the result of a strong asymmetry. The bottom-right inset in figure 5(b) demonstrates a general positive correlation between R^* and the liquid-bridge asymmetry measured by θ . Evidently, the coalescence stage $R^* > 0.3$ indeed has high degrees of asymmetry, roughly corresponding to $\theta > 0.3$.

In figure 5(b), it also seems that all data do not notably exceed the linear regime. To understand the physical R range where the deviation becomes apparent, we can express R^* as $(D_L - D_S)D_L^{-1}R/D_S$, which is generally much smaller than 0.3 for small- Δ cases because $(D_L - D_S)D_L^{-1}$ is rather small. For large Δ , $(D_L - D_S)D_L^{-1}$ approaches unity and the scaling line deflects as R reaches the magnitude of approximately $0.3D_S$, which is rather large. This means that the power-law scaling becomes effectively inaccurate only at large Δ and the bridge's radius is comparable to $0.3D_S$. On the other hand, R has a geometric up-limit of $0.5D_S$, which yields a minimum $\Delta = 2.5$ for one to detect any deviation. This explains why the diversion from $R^2 \sim t$ in figure 4 is observable after a rather late stage of coalescence and when Δ is greater than 3 or so. To understand the time range corresponding to the scaling-law deviation, we can use the asymptotic behaviour $R^{*2} \approx 2t^*$ to obtain the criterion, $t^* > 0.05$. With the calculation of t^* given by (3.9) to (3.10), the criterion can be derived as $t > 0.17\tau_i$ for $\Delta \rightarrow \infty$. For a finite Δ , e.g. $\Delta = 2$, we have $t > 0.85\tau_i$. As $\Delta \rightarrow 1$, the critical time increases dramatically, which makes it physically impossible to break the scaling law.

We last discuss the viscous effect. From our previous theory (Xia *et al.* 2019), the viscous regime for equal-size droplet coalescence occurs for $R/(OhD_S) < 1$. In the present work, as Oh varies from 10^{-3} to 10^{-2} , the viscous regime corresponds to R/D_S being smaller than 10^{-3} – 10^{-2} , for which the evolution process is beyond the resolution of this experiment. Note that during such an early stage the liquid bridge is effectively symmetric, which in turn justifies the extension of the equal-size theory to the unequal-size scenario. Given the limited asymmetry, it can be speculated that there are not substantial differences in the viscous regime between the equal-size and unequal-size situations for the present low- Oh conditions. However, if Oh increases to be $O(10^{-1})$ or higher, the viscous term in the energy balance analysis cannot be ignored, which may render the present model inaccurate. In this case, one may adopt a similar modelling approach to Xia *et al.* (2019) by integrating the Navier–Stokes equation and then incorporating (3.6) to account for the asymmetric bridge movement; this will be explored in our future work.

4. Conclusions

A combined experimental–theoretical investigation was performed to understand the scaling law in the liquid-bridge evolution during the inviscid coalescence of unequal-size droplets. Experimental results suggest that the unequal-size case leads to notably increased prefactor and deviation from the classical 1/2 power-law scaling when the size disparity enlarges. By employing an energy balance analysis, we derived the first theoretical solution for the asymmetric bridge evolution. The resultant model is able to yield the collapse of different-size-ratio data onto a single curve, confirming the relevance of the proposed characteristic length and time scales. Although the solution has a mathematically scaling-free form, its small-time asymptote still recovers the exact 1/2 power-law scaling. This explains why its difference from the power-law scaling is marginal in a wide parameter space of the present experiment. In this sense, this theory can be considered a generalisation of the equal-size scaling law proposed by Eggers *et al.* (1999). However, the emergence of the scaling-free behaviours depends on the liquid bridge being considerably asymmetric, which is satisfied only at sufficiently late coalescence time and large size ratios. We envisage that these new insights will motivate further studies of unequal-size droplet coalescence, in different scenarios related to not only the traditional droplet applications (Eggers *et al.* 2025) but also the emerging technologies of microfluidics (Sun *et al.* 2024) and meta-surface (Xu *et al.* 2023).

Supplementary material. Supplementary material is available at <https://doi.org/10.1017/jfm.2025.353>.

Acknowledgements. We thank Dr Tao Yang and Jiayue Han for their assistance in data processing.

Funding. We acknowledge support from the National Natural Science Foundation of China (nos 52176134 and 12072194), the Research Grants Council of the Hong Kong Special Administrative Region, China (no. CityU 15218820), and the APRC-CityU New Research Initiatives/Infrastructure Support from City University of Hong Kong (no. 9610601).

Declaration of interests. The authors report no conflict of interest.

REFERENCES

- AARTS, D.G.A.L., LEKKERKERKER, H.N.W., GUO, H., WEGDAM, G.H. & BONN, D. 2005 Hydrodynamics of droplet coalescence. *Phys. Rev. Lett.* **95** (16), 164503.
- ANILKUMAR, A.V., LEE, C.P. & WANG, T.G. 1991 Surface-tension-induced mixing following coalescence of initially stationary drops. *Phys. Fluids A* **3** (11), 2587–2591.

- BLANCHETTE, F. 2010 Simulation of mixing within drops due to surface tension variations. *Phys. Rev. Lett.* **105** (7), 074501.
- BURTON, J.C. & TABOREK, P. 2007 Role of dimensionality and axisymmetry in fluid pinch-off and coalescence. *Phys. Rev. Lett.* **98** (22), 224502.
- CASE, S.C. 2009 Coalescence of low-viscosity fluids in air. *Phys. Rev. E* **79** (2), 026307.
- CASE, S.C. & NAGEL, S.R. 2008 Coalescence in low-viscosity liquids. *Phys. Rev. Lett.* **100** (8), 084503.
- DUCHEMIN, L., EGGERS, J. & JOSSERAN, C. 2003 Inviscid coalescence of drops. *J. Fluid Mech.* **487**, 167–178.
- EGGERS, J., LISTER, J.R. & STONE, H.A. 1999 Coalescence of liquid drops. *J. Fluid Mech.* **401**, 293–310.
- EGGERS, J., SPRITTLES, J.E. & SNOEIJER, J.H. 2025 Coalescence dynamics. *Annu. Rev. Fluid Mech.* **57** (1), 61–87.
- FEZZAA, K. & WANG, Y. 2008 Ultrafast x-ray phase-contrast imaging of the initial coalescence phase of two water droplets. *Phys. Rev. Lett.* **100** (10), 104501.
- GRABOWSKI, W.W. & WANG, L.-P. 2013 Growth of cloud droplets in turbulent environment. *Annu. Rev. Fluid Mech.* **45** (1), 293–324.
- GROSS, M., STEINBACH, I., RAABE, D. & VARNIK, F. 2013 Viscous coalescence of droplets: a lattice Boltzmann study. *Phys. Fluids* **25** (5), 052101.
- HACK, M.A., TEWES, W., XIE, Q., DATT, C., HARTH, K., HARTING, J. & SNOEIJER, J.H. 2020 Self-similar liquid lens coalescence. *Phys. Rev. Lett.* **124** (19), 194502.
- KAVEHPOUR, H.P. 2015 Coalescence of drops. *Annu. Rev. Fluid Mech.* **47** (1), 245–268.
- KEISER, L., BENSE, H., COLINET, P., BICO, J. & REYSSAT, E. 2017 Marangoni bursting: evaporation-induced emulsification of binary mixtures on a liquid layer. *Phys. Rev. Lett.* **118** (7), 074504.
- LIU, D., ZHANG, P., LAW, C.K. & GUO, Y. 2013 Collision dynamics and mixing of unequal-size droplets. *Intl J. Heat Mass Transfer* **57** (1), 421–428.
- LOHSE, D. 2022 Fundamental fluid dynamics challenges in inkjet printing. *Annu. Rev. Fluid Mech.* **54** (1), 349–382.
- PAULSEN, J.D. 2013 Approach and coalescence of liquid drops in air. *Phys. Rev. E* **88** (6), 063010.
- PAULSEN, J.D., BURTON, J.C. & NAGEL, S.R. 2011 Viscous to inertial crossover in liquid drop coalescence. *Phys. Rev. Lett.* **106** (11), 114501.
- PAULSEN, J.D., CARMIGNIANI, R., KANNAN, A., BURTON, J.C. & NAGEL, S.R. 2014 Coalescence of bubbles and drops in an outer fluid. *Nat. Commun.* **5** (1), 3182.
- POKLUDA, O., BELLEHUMEUR, C.T. & VLACHOPOULOS, J. 1997 Modification of frenkel’s model for sintering. *AIChE J.* **43** (12), 3253–3256.
- POTHIER, J.C. & LEWIS, L.J. 2012 Molecular-dynamics study of the viscous to inertial crossover in nanodroplet coalescence. *Phys. Rev. B* **85** (11), 115447.
- QIAN, J. & LAW, C.K. 1997 Regimes of coalescence and separation in droplet collision. *J. Fluid Mech.* **331**, 59–80.
- RAY, S., CHI, Y., ZHANG, P. & CHENG, S. 2023 Head-on collision of unequal-size droplets on a wetting surface. *Phys. Fluids* **35** (2), 022114.
- SPRITTLES, J.E. & SHIKHMURZAEV, Y.D. 2012 Coalescence of liquid drops: different models versus experiment. *Phys. Fluids* **24** (12), 122105.
- SPRITTLES, J.E. & SHIKHMURZAEV, Y.D. 2014 Dynamics of liquid drops coalescing in the inertial regime. *Phys. Rev. E* **89** (6), 063008.
- SUN, K., WANG, T., ZHANG, P. & LAW, C.K. 2015 Non-newtonian flow effects on the coalescence and mixing of initially stationary droplets of shear-thinning fluids. *Phys. Rev. E* **91** (2), 023009.
- SUN, S., LI, S., FENG, W., LUO, J., RUSSELL, T.P. & SHI, S. 2024 Reconfigurable droplet networks. *Nat. Commun.* **15** (1), 1058.
- TANG, C., ZHAO, J., ZHANG, P., LAW, C.K. & HUANG, Z. 2016 Dynamics of internal jets in the merging of two droplets of unequal sizes. *J. Fluid Mech.* **795**, 671–689.
- THORODDSEN, S.T., TAKEHARA, K. & ETOH, T.G. 2005 The coalescence speed of a pendent and a sessile drop. *J. Fluid Mech.* **527**, 85–114.
- VAN DYKE, M. 1964 *Perturbation Methods in Fluid Mechanics*. Academic press, Inc.
- WU, M., CUBAUD, T. & HO, C.-M. 2004 Scaling law in liquid drop coalescence driven by surface tension. *Phys. Fluids* **16** (7), L51–L54.
- XIA, X., HE, C., YU, D., ZHAO, J. & ZHANG, P. 2017 Vortex-ring-induced internal mixing upon the coalescence of initially stationary droplets. *Phys. Rev. Fluids* **2** (11), 113607.
- XIA, X., HE, C. & ZHANG, P. 2019 Universality in the viscous-to-inertial coalescence of liquid droplets. *Proc. Natl. Acad. Sci. USA* **116** (47), 23467–23472.
- XU, H., ZHOU, Y., DANIEL, D., HERZOG, J., WANG, X., SICK, V. & ADERA, S. 2023 Droplet attraction and coalescence mechanism on textured oil-impregnated surfaces. *Nat. Commun.* **14** (1), 4901.

- YAO, W., MARIS, H.J., PENNINGTON, P. & SEIDEL, G.M. 2005 Coalescence of viscous liquid drops. *Phys. Rev. E* **71** (1), 016309.
- ZHANG, P. & LAW, C.K. 2011 An analysis of head-on droplet collision with large deformation in gaseous medium. *Phys. Fluids* **23** (4), 042102.